Post-Print

This is the accepted version of:

The final publication is available at http://dx.doi.org/10.1016/j.compositesb.2016.05.044

Access to the published version may require subscription.

When citing this work, cite the original published paper.

Permanent link to this version
http://hdl.handle.net/11311/995608

Fast Analysis of Non-Symmetric Panels Using Semi-Analytical Techniques

Riccardo Vescovini[*1] and Chiara Bisagni[2]

[1]*Department of Aerospace Science and Technology, Politecnico di Milano, Via La Masa 34, 20156 Milano, Italy*

[2]*Faculty of Aerospace Engineering, Section of Aerospace Structures and Computational Mechanics, Delft University of Technology, Kluyverweg 1, 2629 HS Delft, Netherlands*

Abstract

A semi-analytical approach is presented for the analysis and optimization of laminated panels with non-symmetric lay-ups, and with the possibility of introducing requirements on the buckling load, the postbuckling response and the eigenfrequencies. The design strategy relies on the combined use of semi-analytical techniques for the structural analysis and genetic algorithms for the optimization. The structural analysis is performed with a highly efficient code based on thin plate theory, where the problem is formulated in terms of Airy stress function and out of plane displacement, expanded using trigonometric series. Eigenvalue analyses are performed to determine eigenfrequencies and buckling load, while an arc-length method is adopted for the postbuckling computation. The genetic algorithm is implemented with proper alphabet cardinalities to handle different steps for the angles of orientation, while specific mutation operators are used to guarantee good reliability of the optimization. To show the potentialities of the proposed optimization toolbox, two examples are presented regarding the design of balanced non-symmetric laminates subjected to linear and nonlinear constraints. The accuracy of the semi-analytical predictions is demonstrated by comparison with finite element results and benchmark cases taken from the literature.

Keywords: A. Plates; A. Laminates; B. Buckling; C. Analytical modelling; C. Postbuckling.

Corresponding author. Tel: `+39 02 23998332`, *email address:* `riccardo.vescovini@polimi.it` (Riccardo Vescovini)

1 Introduction

In the past years, many efforts were directed towards the development of analytical and semi-analytical methods for the fast analysis of composite panels [1–3]. In most cases, the methods focused on symmetrically layered structures, thus avoiding the coupling between the in plane and out of plane behaviour of the panel. Relatively few works dealt with non-symmetric lay-ups. Similarly, several design optimization procedure were developed by restricting the design space to the case of symmetric lay-ups. Examples are found in two works of the authors [4, 5], where analytical tools are coupled with genetic algorithms, and symmetric lay-ups are assumed. In order to fully exploit the tailoring opportunities offered by composite materials, novel analysis tools are needed to handle more generic lay-up configurations. In this context, closed-form solution are a useful mean to guarantee computational effectiveness, which is particularly useful when dealing with optimization procedures. However, the complexity of the mechanical couplings characterizing the response of generally layered panels often requires the introduction of several simplifying assumptions. An early work of Chandra [6] presents a single-term solution to analyse un-symmetric panels and is restricted to the case of axially compressed cross-ply configurations. The Ritz method is adopted by Dano and Hyer [7] to study the response of non-symmetric panels during the cooling from the cure temperature. More recently, closed-form solutions were derived by Diaconu and Weaver [8] using a single-term approximation to represent the out of plane displacement and considering compression load. Nie and Liu [9] extended the formulation to account for shear loads and elastic restraints. In both in Refs. [8, 9], the approach is valid for infinitely long panels only, and any mode change or snap through cannot be accounted for. Many of the restrictions necessary to derive closed-form solution can be relaxed by adopting multiple-series solutions. In these cases, the equations can be obtained analytically, but the solution is computed numerically. An example is found in the work of Zhang and Matthews [10], where the Airy stress function and the out of plane displacement are approximated with sine terms or beam eigenfunctions. Zhang at al. [11] proposed a formulation based on Karman-Reissner plate theory and asymptotic series solution to study the buckling and the postbuckling response of non-symmetric plates. In both cases, the governing equations regard the out of plane equilibrium and the strain compatibility. The total number of degrees of freedom is still smaller if compared to finite elements, but significantly higher with respect to closed-form solutions. The present

work presents an efficient semi-analytical approach based on multiple degrees of freedom, able to capture mode-jumping phenomena, and characterized by analysis time comparable to closed-form solutions. The approach, which is developed for non-symmetric plates with finite length and loading conditions of compression and shear, is adopted in the context of a design optimization based on genetic algorithms with linear and nonlinear constraints.

2 Semi-analytical model

The analysis tool is implemented in an efficient Matlab program and is developed for the analysis of flat plates layered with symmetric and non-symmetric stacking sequences. Loading conditions of compression and shear are accounted for.

Differently from the vast majority of papers dealing with plate analysis, the present approach does not consider the plate as a self-standing unit, but as a part of a larger structure. This is the typical situation observed in stringer- and frame-stiffened panels, where the overall structure – the fuselage of an aircraft, for instance – is obtained by the repetition of several, self-similar, structural elements. In many cases, it is still possible to isolate the single plate, but for a non-symmetric panel the behaviour can be significantly different.

A sketch of the structure under investigation is provided in Figure 1(a). The model, which is here used for the linear buckling analysis, is composed of a central plate, highlighted in gray, surrounded by to half-bays along the longitudinal and the transverse direction. The central plate element has dimensions a × b, while the dimension of the overall repeating unit is twice the dimension of the central plate, i.e. 2a × 2b.

It is assumed that the structure undergoes local phenomena, meaning that the buckling modes and the postbuckling deformed pattern are characterized by null out of plane deflections along the boundaries, indicated in the figure as nodal lines, of the different plate elements composing the unit. This assumption stems from the consideration that, in a real structure, stringer and frames would be generally designed to avoid the onset of global deflections. Considering the unit of Figure 1(a) as part of a larger structure, periodic conditions are imposed along the four outer boundaries. More specifically, it is assumed that the rotations and displacements along the outer left edge are equal to those of the right edge, and similarly for the upper and lower edge. Regarding the in plane displacements, the panel is free to expand or contract in both the

3

directions, so that no induced stresses are introduced during the loading process.

In the context of the postlbuckling analysis, the model can be further simplified, as illustrated in Figure 1(b), where only the central plate is accounted for, and the effect of the surrounding structure is recovered by means of equivalent springs.

Thin plate assumption is introduced, and Classical Lamination Theory (CLT) is applied. Referring to the central plate element, a Cartesian coordinate system is taken over the panel midsurface with the x-axis directed along the longitudinal direction, the y-axis along the transverse direction and the z-axis to define a right-handed system. The laminate is layered with an arbitrary number of plies, not necessarily stacked to guarantee the symmetry with respect to the midplane of the panel. The only assumption here introduced is that of balanced laminate, meaning that the presence of a ply at $+\theta$ requires the presence of a ply at $-\theta$. The semi-inverse constitutive law of the laminate is:

$$\begin{Bmatrix} \boldsymbol{\xi} \\ \mathbf{M} \end{Bmatrix} = \begin{bmatrix} \mathbf{a} & \mathbf{e} \\ -\mathbf{e}^{\mathrm{T}} & \mathbf{d} \end{bmatrix} \begin{Bmatrix} \mathbf{N} \\ \mathbf{k} \end{Bmatrix} \tag{1}$$

where $\mathbf{N}$ and $\mathbf{M}$ are the force and moment resultant along the thickness, while $\boldsymbol{\xi}$ and $\mathbf{k}$ are the membrane strains and the curvatures, respectively. The matrices $\mathbf{a}$, $\mathbf{d}$, $\mathbf{e}$ of Eq. (1) are related to the $\mathbf{A}$, $\mathbf{B}$, $\mathbf{D}$ matrices of CLT through the relations:

$$\mathbf{a} = \mathbf{A}^{-1} \qquad \mathbf{e} = -\mathbf{A}^{-1}\mathbf{B} \qquad \mathbf{d} = \mathbf{D} - \mathbf{B}\mathbf{A}^{-1}\mathbf{B} \tag{2}$$

Under the assumption of balanced laminate and using the Voigt notation, the only null terms of Eq. (1) are a_{16} and a_{26}.

2.1   Simplified buckling analysis

In the context of the analysis approach here described, the buckling analysis is conducted for two reasons. Firstly, to obtain an estimate of the buckling load of the structure, and secondly to determine the amount of restraint provided by the surrounding structure to the central panel. As illustrated next, the portion of structure that surrounds the central panel of Figure 1(a) can be condensed to a set of equivalent torsion springs along the plate boundaries. This model reduction allows to perform the postbuckling analysis with a restricted number of degrees of freedom and, consequently, with a reduced computational effort.

Although non-symmetric plates may exhibit a non-bifurcational behaviour [12], the buckling

analysis can be performed by introducing simplifying assumptions with regard to the panel response in the pre-buckling range. In particular, the assumptions regard the pre-buckling out of plane displacement, which is taken as identically null, and the pre-buckling stress distribution, which is constant over the panel domain.

The problem is developed in the context of a variational framework, on the basis of the minimum potential energy principle. The total potential energy of the periodic structure of Figure 1 is written as:

$$\delta\Pi^2 = \sum_{N_e} \left(\frac{1}{2} \int_S \left(\boldsymbol{\xi}^T \mathbf{N} + \mathbf{k}^T \mathbf{M} \right) \, \mathrm{dS} + U_{\mathrm{load}} \right) + P \tag{3}$$

where N_e denotes the number of plates composing the assembly of Figure 1, U_{load} is the variation of strain energy due to the pre-buckling loads, and P is a penalty contribution to enforce the continuity of rotations between adjacent plate elements. The present approach is based on a mixed formulation, where the problem is formulated in terms of the out of plane displacement w and the Airy stress function F. Within this context, the vector of in plane forces per unit length $\mathbf{N}$ is defined as:

$$\mathbf{N}^T = \left\{ F_{,xx} \quad F_{,yy} \quad -F_{,xy} \right\} \tag{4}$$

where the comma followed by an index denotes differentiation with respect to that index. After substituting Eq. (2) into Eq. (5), it is obtained:

$$
\begin{aligned}
\delta\Pi^2 &= \sum_{N_e} \left(\frac{1}{2} \int_S \left(\mathbf{N}^T \mathbf{a} \mathbf{N} + \mathbf{k}^T \mathbf{d} \mathbf{k} \right) \, \mathrm{dS} + U_{\mathrm{load}} \right) + P \\
&= \sum_{N_e} \left(U_{\mathrm{m}} + U_{\mathrm{b}} \right) + U_{\mathrm{load}} + P
\end{aligned}
\tag{5}
$$

It can be observed that the first two terms of Eq. (5) correspond to the membrane and the bending energy, while there are no terms responsible for the expected coupling between in plane and out of plane behaviour. This apparently unexpected behaviour is due to adoption of a mixed approach, but does not imply that any sort of simplifying assumption is introduced. In particular, the functional of Eq. (5) cannot be minimized unless the fulfillment of the compatibility condition is guaranteed a priori. It follows that that buckling condition is here obtained in the form of a constrained minimization problem. In particular, the first variation of the potential energy of Eq. (5) is set to zero, subject to the requirement that the linear compatibility equation, for each

element, is identically satisfied:

$$\delta\left(\delta\Pi^2\right) = 0$$

subject to: $L_L(F, w) = 0$

(6)

where:

$$L_{\mathrm{L}}(F, w) = a_{11}F_{,yyyy} + (2a_{12} + a_{66})\,F_{,xxyy} + a_{22}F_{,xxxx} - e_{21}w_{,xxxx}$$
$$- (e_{11} + e_{22} - 2e_{66})\,w_{,xxyy} - e_{12}w_{,yyyy} - (2e_{26} - e_{61})\,w_{,xxxy} - (2e_{16} - e_{62})\,w_{,xyyy}$$

(7)

The terms a_{ik} and e_{ik} are the components of the in plane compliance and the coupling matrix, respectively.

It is now important to highlight that the functions w and F are not independent each other, but they are related via the compatibility equation $L_{\mathrm{L}}(F, w) = 0$. From the fulfillment of the compatibility requirement, it follows that the expression of F depends on the terms e_{ik} (see Eq. (7)) and, when F is substituted back into Eq. (5), the expected coupling between in plane and out of plane response is recovered.

It is remarked that the present formulation leads to the fulfillment of the compatibility and equilibrium conditions in strong- and weak-form, respectively. Other formulations can be found in the literature based on two-field principles (see, for instance, [2, 13, 14]), where both the conditions are imposed in weak-form. In these cases, the problem is solved as an unconstrained minimization problem, and no a priori enforcement of the compatibility condition is needed.

In the context of the present buckling analysis, the functions F and w are intended as the variation with respect to the pre-buckling condition. Under the assumptions of thin-plate theory, the bending energy is:

$$U_{\mathrm{b}} = \frac{1}{2}\int_{\mathrm{S}}\left(d_{11}w_{,xx}^2 + 2d_{12}w_{,xx}w_{,yy} + d_{22}w_{,yy}^2 + 4d_{66}w_{,xy}^2\right.$$
$$\left. + 4d_{16}w_{,xx}w_{,xy} + 4d_{26}w_{,yy}w_{,xy}\right)\,\mathrm{dS}$$

(8)

where the terms d_{ik} are the components of the reduced bending stiffness. It is worth observing that the coupling terms due to the non-symmetry of the laminate enter in the bending energy expression because the matrix $\mathbf{d}$ is function of $\mathbf{B}$.

The membrane contribution is:

$$U_{\mathrm{m}} = \frac{1}{2}\int_{\mathrm{S}}\left(a_{11}F_{,yy}^2 + 2a_{12}F_{,xx}F_{,yy} + a_{22}F_{,xx}^2 + a_{66}F_{,xy}^2\right)\,\mathrm{dS}$$

(9)

As done for the out of plane displacement, the function F is here intended as the variation with respect to the pre-buckling condition.

The expression for the incremental strain energy relative to the applied loads is:

$$U_{\text{load}} = -\frac{1}{2}\lambda \hat{N}_x \int_S w_{,x}^2 \; \text{dS} + \lambda \hat{N}_{xy} \int_S w_{,x} w_{,y} \; \text{dS} \tag{10}$$

where $\hat{N}_x$ and $\hat{N}_{xy}$ are the pre-buckling forces per unit length and λ is the buckling multiplier. The penalty term of Eq. (5) is obtained as the superposition of two terms as:

$$P = \sum_{i=1}^{N_p} P_{i,\text{long}} + \sum_{i=1}^{N_p} P_{i,\text{trans}} \tag{11}$$

where N_p is the number of penalty terms to be imposed, and $P_{i,\text{trans}}$ and $P_{i,\text{long}}$ are the penalty energy contributions due to the enforcement of the compatibility conditions along the transverse and the longitudinal edges, respectively. The expression of the terms of Eq. (11), relative to the generic plates i and j, is:

$$P_{i,\text{long}} = \frac{1}{2}k_{\text{t}} \int_0^a \left(w_{i,y} - w_{j,y} \right)^2 \; \text{d}x \tag{12}$$

$$P_{i,\text{trans}} = \frac{1}{2}k_{\text{t}} \int_0^b \left(w_{i,x} - w_{j,x} \right)^2 \; \text{d}y \tag{13}$$

where k_{t} is the penalty stiffness, whose value has to be taken sufficiently high to ensure the fulfillment of the compatibility condition. The same strategy was applied in [5, 15], proving to be an efficient and robust approach, insensitive to the value of k_{t} in a wide range of values.

Ritz solution

The stationarity condition of Eq. (6) is imposed referring to the method of Ritz. For each plate element, the out of plane displacement is approximated with a double series of sine terms as:

$$w = \sum_{mn}^{RS} q_{mn} \sin\frac{m\pi x}{a} \sin\frac{n\pi y}{b} = \mathbf{N}^{\text{w}} \mathbf{q}_i \tag{14}$$

The unknown amplitudes q_{mn} of Eq. (14) are collected in the column vector $\mathbf{q}_i$ of dimensions R×S defined as $\mathbf{q}_i = \{q_{11} \cdots q_{1S} q_{21} \cdots q_{2S} \cdots q_{RS}\}^{\text{T}}$. The matrix of the shape functions $\mathbf{N}^w$ is defined accordingly.

The expansion of Eq. (14) guarantees that the buckling mode is null at the boundaries, meaning that it is characterized by nodal lines at the intersection between the elements composing the

structure of Figure 1.

To ensure the respect of the compatibility requirement of Eq. (6), the Airy stress function is expanded as the sum of two contributions:

$$F(x, y) = G(x, y) + H(x, y) \tag{15}$$

where the functions G and H describe the variation of the in-plane forces with respect to the pre-buckling condition.

The expression of the functions G and H is sought in the form:

$$G(x, y) = \sum_{mn=1}^{RS} g_{mn} \cos \frac{m\pi x}{a} \cos \frac{n\pi y}{b} = \mathbf{N}^g \mathbf{g} = \mathbf{N}^{\mathrm{g}} \mathrm{diag}[\mathbf{b}^{\mathrm{g}}] \mathbf{q}_{\mathrm{i}} \tag{16}$$

$$H(x, y) = \sum_{mn=1}^{RS} h_{mn} \sin \frac{m\pi x}{a} \sin \frac{n\pi y}{b} = \mathbf{N}^h \mathbf{h} = \mathbf{N}^{\mathrm{h}} \mathrm{diag}[\mathbf{b}^{\mathrm{h}}] \mathbf{q}_{\mathrm{i}} \tag{17}$$

where the relation between the amplitudes g_{mn}, h_{mn} and q_{mn} is given by the vectors $\mathbf{b}^{\mathrm{g}}$ and $\mathbf{b}^{\mathrm{h}}$, whose expression is obtained by substitution of Eqs. (16) and (17) into the compatibility condition of Eq. (6). The generic component b_i^{g} of the vector $\mathbf{b}^{\mathrm{g}}$ is:

$$b_i^{\mathrm{g}} = \frac{(2e_{26} - e_{61}) \left(\frac{m}{a}\right)^3 \frac{n}{b} + (2e_{16} - e_{62}) \frac{m}{a} \left(\frac{n}{b}\right)^3}{a_{11} \left(\frac{n}{b}\right)^4 + (2a_{12} + a_{66}) \left(\frac{mn}{ab}\right)^2 + a_{22} \left(\frac{m}{a}\right)^4} \tag{18}$$

Similarly, the vector $\mathbf{b}^{\mathrm{h}}$ has components:

$$b_i^{\mathrm{h}} = \frac{e_{21} \left(\frac{m}{a}\right)^4 + (e_{11} + e_{22} - 2e_{66}) \left(\frac{mn}{ab}\right)^2 + e_{12} \left(\frac{n}{b}\right)^4}{a_{11} \left(\frac{n}{b}\right)^4 + (2a_{12} + a_{66}) \left(\frac{mn}{ab}\right)^2 + a_{22} \left(\frac{m}{a}\right)^4} \tag{19}$$

As observed in Eqs. (16) and (17), the unknown amplitudes of the Airy stress function can be expressed in terms of the amplitudes $\mathbf{q}_i$, which are the only unknown of the problem. In the context of the buckling analysis, the relation is linear.

It is also observed that Eqs. (18) and (19) depend on the laminate constitutive terms e_{ik}, which are responsible for the coupled behaviour between in plane and out of plane response.

The bending energy is directly computed by substitution of Eq. (14) into Eq. (8), and is written as:

$$U_{\mathrm{b}} = \frac{1}{2} \mathbf{q}_i^{\mathrm{T}} \mathbf{K}_{\mathrm{b}} \mathbf{q}_i \tag{20}$$

8

where $\mathbf{K}_b$ is the reduced bending stiffness matrix.

After substitution of Eqs. (16) and (17) into Eq. (9), the membrane energy can be written as a quadratic term in the unknown $\mathbf{q}$:

$$U_{\mathrm{m}} = \frac{1}{2}\mathbf{g}^{\mathrm{T}}\boldsymbol{\alpha}^{\mathrm{gg}}\mathbf{g} + \frac{1}{2}\mathbf{h}^{\mathrm{T}}\boldsymbol{\alpha}^{\mathrm{hh}}\mathbf{h} = \\ = \frac{1}{2}\mathbf{q}_i^{\mathrm{T}}\mathbf{K}_{\mathrm{m}}^{\mathrm{lin}}\mathbf{q}_i \tag{21}$$

where the matrices $\boldsymbol{\alpha}^{\mathrm{gg}}$, $\boldsymbol{\alpha}^{\mathrm{hh}}$ collect the coefficients resulting from the analytical integration of Eq. (9) and the membrane stiffness matrix $\mathbf{K}_{\mathrm{m}}^{\mathrm{lin}}$ is:

$$\mathbf{K}_{\mathrm{m}}^{\mathrm{lin}} = \mathrm{diag}[\mathbf{b}^{\mathrm{g}}]^{\mathrm{T}}\boldsymbol{\alpha}^{\mathrm{gg}}\mathrm{diag}[\mathbf{b}^{\mathrm{g}}] + \mathrm{diag}[\mathbf{b}^{\mathrm{h}}]^{\mathrm{T}}\boldsymbol{\alpha}^{\mathrm{hh}}\mathrm{diag}[\mathbf{b}^{\mathrm{h}}] \tag{22}$$

After substitution of Eq. (14) into Eq. (10), the strain energy increment due to the pre-buckling load is:

$$U_{\mathrm{load}} = \lambda\frac{1}{2}\mathbf{q}_i^{\mathrm{T}}\left(\mathbf{K}_{\mathrm{c}} + \mathbf{K}_{\mathrm{s}}\right)\mathbf{q}_i \tag{23}$$

In a similar way, the out of plane displacement of Eq. (14) is substituted into Eqs. (12) and (13). Observing that the penalty terms involve the deflection of different plate elements, the corresponding strain energy is written in terms of the global vector of unknowns $\mathbf{q}$:

$$P = \frac{1}{2}\mathbf{q}^{\mathrm{T}}\mathbf{P}\mathbf{q} \tag{24}$$

where the vector of global unknowns is defined as:

$$\mathbf{q} = \left\{\mathbf{q}_1^{\mathrm{T}} \quad \mathbf{q}_2^{\mathrm{T}} \quad \mathbf{q}_3^{\mathrm{T}} \quad \mathbf{q}_4^{\mathrm{T}}\right\}^{\mathrm{T}} \tag{25}$$

After substitution of Eqs. (20), (21) and (23) into Eq. (5), the buckling eigenvalue problem is obtained as:

$$\delta\left(\delta\Pi^2\right) = \delta\mathbf{q}^{\mathrm{T}}\left(\hat{\mathbf{K}} + \lambda\hat{\mathbf{K}}_{\mathrm{load}}\right)\mathbf{q} = 0 \tag{26}$$

where the stiffness matrix $\mathbf{K}$ and the loading stiffness matrix $\mathbf{K}_{\mathrm{load}}$ are given by:

$$\hat{\mathbf{K}} = \mathrm{diag}[\mathbf{K}_{\mathrm{b}}] + \mathrm{diag}[\mathbf{K}_{\mathrm{m}}^{\mathrm{lin}}] + \mathbf{P} \tag{27}$$

$$\hat{\mathbf{K}}_{\mathrm{load}} = \mathrm{diag}[\mathbf{K}_{\mathrm{c}} + \mathbf{K}_{\mathrm{s}}] \tag{28}$$

The minimum among the positive eigenvalues obtained from the solution of the eigenvalue problem of Eq. (28) is the multiplier of the pre-buckling condition. The corresponding eigenvector

9

determines the buckling shape of the structure.

It is worth noting that the free vibration problem can be easily derived from Eq. (26) by replacing the loading stiffness with the mass matrix. In this case, the corresponding eigenvalue problem reads:

$$\delta \mathbf{q}^{\mathrm{T}} \left(-\omega^2 \hat{\mathbf{M}} + \hat{\mathbf{K}} \right) \mathbf{q} = 0 \tag{29}$$

Condensation of the surrounding structure

Thanks to the symmetry of the problem, the portion of structure around the central plate can be condensed, making it possible a reduction of the problem size for the postbuckling analysis. Due the symmetry of the buckling modes, the following relation holds between the eigenvector of the central element, here denoted with the subscript element 1, and those relative to the surrounding plates:

$$\mathbf{q}_i = \pm \mathbf{q}_1 \quad \text{with } i \neq 1 \tag{30}$$

The relation of Eq. (30) illustrates that the buckling modes of the central element is always equal or opposite to the deflection of the surrounding elements. According to Eq. (30), the global vector of the degrees of freedom can then be related to the degrees of freedom of the element 1 as:

$$\mathbf{q} = \begin{bmatrix} \mathbf{I} \\ \mathbf{T}_2 \\ \mathbf{T}_3 \\ \mathbf{T}_4 \end{bmatrix} \mathbf{q}_1 = \mathbf{T} \mathbf{q}_1 \tag{31}$$

where the transformation matrices $\mathbf{T}_i$ have ± 1 terms along the diagonal, and are determined on the basis of the results of the buckling eigenvalue analysis.

The relation of Eq. (31) provides the transformation law to reduce the penalty term $\mathbf{P}$ to the degrees of freedom of the central plate element. Indeed, from Eqs. (26) and (27), it can be observed that:

$$\delta \mathbf{q}^{\mathrm{T}} \hat{\mathbf{K}} \mathbf{q} = 4 \delta \mathbf{q}_1^{\mathrm{T}} \left(\mathbf{K}_{\mathrm{b}} + \mathbf{K}_{\mathrm{m}}^{\mathrm{lin}} + \mathbf{K}_{\mathrm{k}} \right) \mathbf{q}_1 \tag{32}$$

where:

$$\mathbf{K}_{\mathrm{k}} = \frac{1}{4} \mathbf{T}^{\mathrm{T}} \mathbf{P} \mathbf{T} \tag{33}$$

The expression of Eq. (32) illustrates that the minimization of the elastic energy stored in the structure of Figure 1 is identical to the minimization of the energy stored in the central plate,

provided that the penalty term is condensed according to Eq. (33). This term, which is quadratic in $\mathbf{q}$, accounts for the fact that the deflection of the central plate influences the deflection of the surrounding structure. It can be thought as the energy associated to the deflection of equivalent torsion springs, distributed along the boundaries of the central plate element, whose strain energy is:

$$U_{\mathrm{k}} = \frac{1}{2}\mathbf{q}_1^{\mathrm{T}}\mathbf{K}_{\mathrm{k}}\mathbf{q}_1 \qquad (34)$$

2.2 Postbuckling analysis

Consistently with the approach adopted for the buckling analysis, the postbuckling formulation is developed within a variational framework. On the basis of the results obtained with the linear buckling analysis, the model is restricted to the central plate of the periodic structure, illustrated in Figure 1(b), and the effect of the surrounding portion of structure is recovered by accounting for the quadratic energy term of Eq. (33).

The nonlinear expression of the total potential energy is now considered. In particular, the expression reads:

$$\Pi = U_{\mathrm{b}} + U_{\mathrm{m}} + U_{\mathrm{k}} + V_{\mathrm{c}} + V_{\mathrm{s}} \qquad (35)$$

where U_{b} and U_{m} are the bending and the membrane energies, while the contribution U_{k} accounts for the portion of structure around the central plate, according to Eq. (34). The terms V_{c} and V_{s} of Eq. (35) are the potentials of the compressive and shear loads. Referring to Eq. (35), the equilibrium configuration is obtained by solving of the following constrained minimization problem:

$$\begin{aligned} &\delta\Pi = 0 \\ &\text{subject to: } L_{\mathrm{L}}(F, w) + \frac{1}{2}L_{\mathrm{NL}}\left(w, w + 2w_0\right) = 0 \end{aligned} \qquad (36)$$

where the function w_0 defines the panel initial imperfection. The constraint of Eq. (36) is the compatibility requirement, expressed in terms of the linear operator of Eq. (7) and the nonlinear operator L_{NL}, whose expression is:

$$L_{\mathrm{NL}}(w, w + 2w_0) = w_{,xx}\left(w + 2w_0\right)_{,yy} - 2w_{,xy}\left(w + 2w_0\right)_{,xy} + w_{,yy}\left(w + 2w_0\right)_{,xx} \qquad (37)$$

The membrane and the bending contributions, expressed in terms of Airy stress function and out of plane displacement, are given by Eqs. (8) and (9). It is worth noting that the functions w

and F are, in this context, the actual out of plane displacement and Airy stress functions, and not the variation with respect to the pre-buckling configuration, as for the buckling analysis. Following Refs. [16–18], the potential of the compression load is:

$$V_{\mathrm{c}} = b\overline{N}_x\Delta\overline{U} \tag{38}$$

where $\overline{N}_x$ is the average stress resultant during the loading phase, taken positive in compression, and $\Delta\overline{U}$ is the average end shortening of the panel, defined as:

$$\Delta\overline{U} = \frac{\overline{N}_x}{b}\int_{\mathrm{S}}\left(-\xi_{xx} + \frac{1}{2}w_{,x}^2 + w_{0,x}w_{,y} + w_{0,y}w_{,x}\right)\,\mathrm{dS} \tag{39}$$

The potential of the shear load is expressed as:

$$V_{\mathrm{s}} = \overline{N}_{xy}\int_{\mathrm{S}}\left(w_{,x}w_{,y} + w_{,x}w_{0,y} + w_{,y}w_{0,x}\right)\,\mathrm{dS} \tag{40}$$

Ritz solution

The postbuckling formulation is expressed as function of the unknowns w and F. The out of plane displacement w is expanded according to Eq. (14), while the Airy stress function is obtained, as illustrated next, by imposing the solution of the nonlinear compatibility requirement of Eq. (36). In addition, the nonlinear formulation accounts for the presence of initial imperfections, which are approximated as a double sine expansion:

$$w_0 = \sum_{mn}^{RS} q_{mn}^0 \sin\frac{m\pi x}{a}\sin\frac{n\pi y}{b} = \mathbf{N}^w\mathbf{q}^0 \tag{41}$$

where the amplitudes $\mathbf{q}^0$ are known a priori to achieve the desired geometric imperfection shape. To ensure the respect of the compatibility requirement of Eq. (36), the Airy stress function is expressed as the sum of five contributions:

$$F(x,y) = -\frac{1}{2}\overline{N}_xy^2 - \overline{N}_{xy}xy + F_{\mathrm{NL}}(x,y) + G(x,y) + H(x,y) \tag{42}$$

The first two terms of Eq. (42) are responsible for the uniform stress distribution over the panel, while the functions G, H and F_{NL} describe the stress redistribution due to the panel deflection. In particular, the terms G and H are those reported in Eqs. (16) and (17) and depend linearly on the deflection amplitude $\mathbf{q}$. The function F_{NL} is relative to the postbuckling nonlinear stress redistribution, and its expression is:

$$F_{\mathrm{NL}}(x,y) = \sum_{mn=0}^{2R,2S} f_{mn}\cos\frac{m\pi x}{a}\cos\frac{n\pi y}{b} = \mathbf{N}^{\mathrm{NL}}\mathbf{f} \tag{43}$$

12

The vector of amplitudes $\mathbf{f}$ can be expressed in terms of $\mathbf{q}$ by substitution of Eqs. (14), (41) and (43) into the compatibility requirement of Eq. (36). It can be demonstrated that the generic coefficient f_i of the vector $\mathbf{f}$ is a quadratic function of the deflection amplitudes $\mathbf{q}$, and is obtained by:

$$f_i = \mathbf{q}^{\mathrm{T}} \mathbf{B}_i^{\mathrm{sym}} \left(\frac{1}{2}\mathbf{q} + \mathbf{q}^0 \right) \tag{44}$$

where $\mathbf{B}_i^{\mathrm{sym}} = \mathbf{B}_i + \mathbf{B}_i^{\mathrm{T}}$, and $\mathbf{B}_i$ is a matrix of scalar coefficients, built according to the approach reported in [16, 18].

As observed in Eqs. (16), (17) and (44), the unknown amplitudes of the Airy stress function can be expressed in terms of the amplitudes $\mathbf{q}$, which are the only unknown of the problem. After substitution of Eq. (42) into Eq. (9), the membrane energy can be written as the sum of three contributions:

$$U_{\mathrm{m}} = U_{\mathrm{m}}^{\mathrm{lin}} + U_{\mathrm{m}}^{\mathrm{nl,ff}} + U_{\mathrm{m}}^{\mathrm{nl,fg}} \tag{45}$$

The first term of Eq. (45) is quadratic in $\mathbf{q}$ and is null for symmetric panels. The second and the third terms are quartic and cubic in $\mathbf{q}$, respectively.

After collecting the coefficients obtained from the analytical integration of the membrane energy in the matrices $\boldsymbol{\alpha}^{\mathrm{ff}}$ and $\boldsymbol{\alpha}^{\mathrm{fg}}$, it is obtained:

$$U_{\mathrm{m}}^{\mathrm{lin}} = \frac{1}{2}\mathbf{q}^{\mathrm{T}}\mathbf{K}_{\mathrm{m}}^{\mathrm{lin}}\mathbf{q} \qquad U_{\mathrm{m}}^{\mathrm{nl,ff}} = \frac{1}{2}\mathbf{f}^{\mathrm{T}}\boldsymbol{\alpha}^{\mathrm{ff}}\mathbf{f} \qquad U_{\mathrm{m}}^{\mathrm{nl,fg}} = \frac{1}{2}\mathbf{f}^{\mathrm{T}}\boldsymbol{\alpha}^{\mathrm{fg}}\mathbf{g} \tag{46}$$

The bending energy is directly computed by substitution of Eq. (14) into Eq. (8), and the corresponding discrete expression is reported in Eq. (20).

Regarding the potential of the compression load, the contribution is obtained by substitution of Eq. (14) into Eq. (38), and is written as:

$$V_{\mathrm{c}} = \overline{N}_x aba_{11} + \frac{1}{2}\mathbf{q}^{\mathrm{T}}\mathbf{K}_{\mathrm{c}}\left(\mathbf{q} + 2\mathbf{q}^0\right) \tag{47}$$

where the matrix $\mathbf{K}_c$ collects the numerical coefficients obtained from the closed-form integration of the integrals involved in the expressions of the potential of the external loads.

The potential of the shear loads reads:

$$V_{\mathrm{s}} = \frac{1}{2}\mathbf{q}^{\mathrm{T}}\mathbf{K}_{\mathrm{s}}\left(\mathbf{q} + 2\mathbf{q}^0\right) \tag{48}$$

where $\mathbf{K}_{\mathrm{s}}$ is determined by integrating Eq. (40) analytically.

Arc-length solution procedure

The nonlinear equations governing the postbuckling response of the panel are derived following the approach discussed in Refs. [10, 11], where a perturbation arc length approach is implemented. The main advantage of this solution scheme relies in its robustness to capture mode changes or snap through. This feature is particularly interesting in the context of an optimization procedure, where it becomes mandatory to guarantee that each of the structural analysis terminates without convergence issues. The set of nonlinear equations governing the postbuckling behaviour of the panel are derived in rate form as:

$$\frac{\partial \Pi_{,\eta}}{\partial \mathbf{q}} = \mathbf{K}\mathbf{q}_{,\eta} + \mathbf{s}\Lambda_{,\eta} = \mathbf{0} \tag{49}$$

where Λ and η are the load and the rate parameters, respectively.

Due to the introduction of the load parameter Λ, the discrete problem is augmented by introducing a constraint equation. Following [19], the augmented problem reads:

$$\begin{cases} \mathbf{K}\mathbf{q}_{,\eta} + \mathbf{s}\Lambda_{,\eta} = \mathbf{0} \\ \Lambda_{,\eta} + \mathbf{q}^{\mathrm{T}}\mathbf{q} = 1 \end{cases} \tag{50}$$

The first term in the right hand side of Eq. (49) is the tangent stiffness matrix, while the second contribution is the incremental load vector, which are defined as:

$$\mathbf{K} = \frac{\partial^2 \Pi}{\partial \mathbf{q}^2} \tag{51}$$

$$\mathbf{s} = \frac{\partial^2 \Pi}{\partial \mathbf{q} \partial \Lambda} \tag{52}$$

The tangent stiffness matrix $\mathbf{K}$ is obtained as the sum of two contributions, a linear term independent on the configuration, and a nonlinear term which is function of the current deformation. The matrix is so re-written as:

$$\mathbf{K} = \mathbf{K}^{\mathrm{lin}} + \mathbf{K}_{\mathrm{m}}^{\mathrm{nl}}(\mathbf{q}) \tag{53}$$

where the linear contribution is derived from:

$$\mathbf{K}^{\mathrm{lin}} = \frac{\partial^2 \left(U_{\mathrm{b}} + U_{\mathrm{m}}^{\mathrm{lin}} + U_{\mathrm{k}} + V_{\mathrm{c}} + V_{\mathrm{s}} \right)}{\partial \mathbf{q}^2} =$$
$$= \mathbf{K}_{\mathrm{b}} + \mathbf{K}_{\mathrm{m}}^{\mathrm{lin}} + \mathbf{K}_{\mathrm{k}} + \Lambda \left(\mathbf{K}_{\mathrm{c}} + \mathbf{K}_{\mathrm{s}} \right) \tag{54}$$

14

The second contribution to the tangent stiffness matrix is due to the nonlinear terms of the membrane energy, as observed in Eqs. (45) and (46). The two terms are written as:

$$\mathbf{K}_\mathrm{m}^\mathrm{nl} = \mathbf{K}_\mathrm{m}^\mathrm{nl,ff} + \mathbf{K}_\mathrm{m}^\mathrm{nl,fg} \tag{55}$$

where $\mathbf{K}_m^\mathrm{nl,ff}$ is obtained by recalling the second of Eq. (46). In particular, it is:

$$\begin{aligned} \mathbf{K}_\mathrm{m}^\mathrm{nl,ff} = \frac{\partial^2 \Pi_\mathrm{m}^\mathrm{nl,ff}}{\partial \mathbf{q}^2} = \\ = \sum \frac{\partial f_i}{\partial \mathbf{q}} \frac{\partial^2 \Pi_m^\mathrm{nl,ff}}{\partial f_i \partial f_j} \frac{\partial f_j}{\partial \mathbf{q}} + \sum \frac{\partial \Pi_m^\mathrm{nl,ff}}{\partial f_i} \frac{\partial^2 f_i}{\partial \mathbf{q}^2} \end{aligned} \tag{56}$$

From the expressions of Eqs. (44) and (46), the nonlinear part of the stiffness due the membrane energy is obtained as:

$$\mathbf{K}_\mathrm{m}^\mathrm{nl,ff} = \sum_{i,j=0}^{2R,2S} \mathbf{B}_i^\mathrm{sym} \left(\mathbf{q} + \mathbf{q}^0 \right) \alpha_{ij}^\mathrm{ff} \left(\mathbf{q} + \mathbf{q}^0 \right)^\mathrm{T} \mathbf{B}_i^\mathrm{sym} + v_i \mathbf{B}_i^\mathrm{sym} \tag{57}$$

where the term v_i is the i-th component of the vector $\mathbf{v}$, obtained as:

$$\mathbf{v} = \boldsymbol{\alpha}^\mathrm{ff} \mathbf{f} \tag{58}$$

and the components of the vector $\mathbf{f}$ are obtained according to Eq. (44). The second contribution to the nonlinear part of the tangent stiffness matrix regards the coupling between the functions F and G, and is derived as:

$$\begin{aligned} \mathbf{K}_\mathrm{m}^\mathrm{nl,fg} = \frac{\partial^2 \Pi_\mathrm{m}^\mathrm{nl,fg}}{\partial \mathbf{q}^2} = \\ = \sum_{i=0}^{2R \times 2S} \sum_{j=1}^{R \times S} \frac{\partial f_i}{\partial \mathbf{q}} \frac{\partial^2 \Pi_\mathrm{m}^\mathrm{nl,fg}}{\partial f_i \partial g_j} \frac{\partial g_j}{\partial \mathbf{q}} + \frac{\partial g_j}{\partial \mathbf{q}} \frac{\partial^2 \Pi_\mathrm{m}^\mathrm{nl,fg}}{\partial g_i \partial f_j} \frac{\partial f_j}{\partial \mathbf{q}} + \sum_{i=0}^{2R \times 2S} \frac{\partial \Pi_\mathrm{m}^\mathrm{nl,fg}}{\partial f_i} \frac{\partial^2 f_i}{\partial \mathbf{q}^2} = \\ = \tilde{\mathbf{K}} + \tilde{\mathbf{K}}^\mathrm{T} + w_i \mathbf{B}_i^\mathrm{sym} \end{aligned} \tag{59}$$

where the matrix $\tilde{\mathbf{K}}$ is defined as:

$$\tilde{\mathbf{K}} = \sum_{i=0}^{2R \times 2S} \mathbf{B}_i^\mathrm{sym} \left(\mathbf{q} + \mathbf{q}^0 \right) \alpha_\mathrm{ij}^{fg} \tilde{\mathbf{b}}_j^\mathrm{g} \tag{60}$$

The row vector $\tilde{\mathbf{b}}_j^g$ is the j-th row of the matrix $\mathrm{diag}[\mathbf{b}^\mathrm{g}]$, and the term w_i of Eq. (59) is the i-th component of the vector $\mathbf{w}$, obtained as:

$$\mathbf{w} = \boldsymbol{\alpha}^\mathrm{fg} \mathbf{B}^\mathrm{g} \mathbf{q} \tag{61}$$

The derivation of the incremental load vector s is straightforward, and is obtained as:

$$\mathbf{s} = \frac{\partial^2 \left(V_\mathrm{c} + V_\mathrm{s} \right)}{\partial \mathbf{q} \partial \Lambda} = \Lambda \left(\mathbf{K}_\mathrm{c} + \mathbf{K}_\mathrm{s} \right) \left(\mathbf{q} + \mathbf{q}^0 \right) \tag{62}$$

15

3   Optimization algorithm

The optimization process is here performed with a code based on genetic algorithms (GA) modified for the design of composite structures. In particular, new genetic operators are introduced to improve the reliability of the code, on the basis of the investigations conducted by Nagendra et al. [20]. The code is implemented in Matlab language, and can be easily linked to the structural analysis tool described in the previous section. As input data, the optimization routine requires the definition of the number of variables, their range, the cardinality of the alphabet to encode the variables, the functions to compute the fitness and the constraints, the penalty terms associated to each of the constraints, and the parameters relative to the mutation operators. The optimization process begins with the initial construction of a pool of candidates, i.e. the first generation of individuals. The quality of each of the individuals, i.e. the first set of possible designs, is initially established by evaluation of their fitness function, including the penalty contribution due to the constraints that the design is required to satisfy.

Depending on the fitness of each single individual, the members of the first generation are sorted and submitted to the selection process, which can be based on different criteria. In the present implementation, a probability is attributed to the individuals based on their ranking: the fittest members are those with highest chance of being selected for becoming parents, while the less fit are unlikely to be selected. In any case, a non null probability is associated to all the members of the pool, so that even the less fit designs have a chance of becoming parents. This aspect, together with the other mutation operators, plays an important role in guaranteeing that the optimization process does not converge to local minima.

For each couple of parents, new individuals are created by applying the crossover operator. It consists in recombining the information encoded in the chromosomes of the selected parents to obtain a new design. The single point crossover is here considered among the various implementations proposed in the literature.

The mutation operator is applied just after the application of the crossover. In this case, mutation is performed by means of four different operators. The last step of the genetic process consists in the insertion of the offspring into the new generation. The optimization code allows to define an arbitrary number of elite members. The overall procedure is repeated until a convergence criterion is met. Different criteria are implemented in the code, consisting in the maximum

number of generations, fitness functions evaluations and generations with no improvement of the best individuals.

3.1 Chromosome encoding

Each individual of the population is represented by a chromosome, which is responsible for encoding the genetic information. To this aim, different alphabets can be used, the binary representation being one of the most common. In the context of stacking sequence optimization, design variables are represented by the angles of orientation of each ply, and the problem becomes an integer optimization problem (or a mixed-integer problem if, in addition, other real variables are involved). A suitable strategy for encoding the angles of orientation of a laminate consists in the use of alphabets of higher cardinality, where an integer number is associated to each ply angle. The cardinality of the alphabet is then dependent on the number of plies made available for the design. For instance, a 3-ary alphabet is considered if the plies can be oriented at $0°$, $45°$, $90°$.

In the present work, alphabets of cardinality of 7 and 13 are considered, in order to allow the design of panels with plies oriented from $0°$ to $90°$, with steps of $15°$ and $7.5°$, respectively. In the first case, the value 0 means $0°$, 1 means $15°$, 2 stands for $30°$, and so on. Furthermore, the pool of available design is restricted to that of balanced laminates. To this aim the chromosome encoding is performed such that each gene denotes a couple of plies oriented at $\pm\theta$. This strategy is inspired by the results reported in Ref. [21], where it was demonstrated that a penalty approach is not efficient to enforce the balance constraint, adding noise to the fitness function. An example of chromosome decoding is reported in Eq. (63) assuming the case of cardinality 7:

$$[303441] \rightarrow [\pm45°/\pm0°/\pm45°/\pm60°/\pm60°/\pm15°] \tag{63}$$

It is remarked that the optimization code implemented allows the introduction of any encoding rule, so that the assumption of balanced laminates, or the use of different alphabets can be easily modified. Laminates with a variable number of plies are handled by associating an integer value to a dummy ply.

3.2 Genetic operators

The crossover operator is here implemented in its one-point version, meaning that one single cut point is randomly chosen for each of the two parents. The crossover operator is slightly modified when a variable number of plies is allowed. In this case, the chromosome is firstly resorted by packing all the N empty plies in the first N genes, and the crossover cut point is forced to fall in the remaining genes. Regarding the mutation operators, specific operators are implemented to improve the reliability of the procedure, as demonstrated in Ref. [20].

The first operator is the ply swap, consisting in a random selection and the swap of two plies. The use of this operator is motivated by the fact that inner and outer plies have different influences on the bending stiffness of the laminate. Therefore the external plies reach convergence faster than the internal ones.

A second mutation operator is the angle ply mutation that consists in randomly picking one gene and altering its value with any of the possible angles. In presence of a variable number of plies, two more operators are available, namely the ply addition and ply deletion operators. Their application consists in the addition of a randomly oriented ply, or the deletion of a ply. It is noted that ply addition and deletion operators are applied to the innermost ply, the less influential in terms of laminate bending stiffness. With this approach, abrupt changes of laminate bending stiffness, which may have a too drastic impact on the mutated individual, are avoided.

After crossover and mutation operations, the new generation is created applying an elitist selection. Elitism is a well know strategy to improve the convergence properties of the genetic algorithm. On one hand, it has the effect of speeding-up the convergence to a maximum, but on the other hand it weakens the explorative ability of the method in the design space. Elitism is here implemented by taking the fittest individual. Elite members are passed intact to the following generation in order to guarantee that the fittest individuals are not lost due to the application of the genetic operators during crossover and mutation.

The selection is performed with a tournament of variable size. The effect of enlarging the tournament size is to increase the selective pressure, with the risk of reducing the diversity in the new population. For this reason, a size of 2 is here considered.

4   Analysis results

Before illustrating the results of the optimization, the quality of the semi-analytical predictions is assessed by presenting the comparison with results available in the literature and numerical simulations.

To this aim, the commercial finite element code Abaqus is adopted, and the finite element meshes are realized by modeling the full representative unit of Figure 1. The four outer sides of the structure are subjected to periodic boundary conditions. In particular, the two transverse edges are forced to undergo equal translations along the z direction and rotations around the x-axis, and are forced to remain straight. The longitudinal edges are subjected to a constraint equation forcing the nodal degrees of freedom to display equal translations along z and rotations around y. Regarding the translation along the x direction, the axial load is introduced by defining a constraint equation:

$$u_x^{\text{upper}} - u_x^{\text{lower}} = \Delta U \tag{64}$$

where u_x^{upper} and u_x^{lower} are the set of nodes belonging to the upper and lower edges of the panel, respectively, while ΔU is the imposed shortening.

In a similar fashion, shear loads are introduced using a constraint equation defined as:

$$u_y^{\text{upper}} - u_y^{\text{lower}} = \Delta V \tag{65}$$

The finite element analyses are conducted by performing a preliminary eigenvalue analysis to determine the bifurcation buckling load. The nonlinear response is studied with a quasi-static nonlinear step, assuming an initial imperfection equal to the first buckling mode with maximum nondimensional amplitude w_0/t of 1%. The mesh is realized using four node S4R elements, whose dimension is set, case by case, to ensure the convergence of the results.

4.1   Comparison with literature

A first set of results deals with the analysis of long non-symmetric plates studied by Diaconu and Weaver [8], whose closed-form solutions are used for comparison purposes.

The material is graphite epoxy, whose elastic properties are $E_{11}/E_{22}=20$, $G_{12}/E_2=0.5$ and $\nu_{12}=0.25$. The plates have aspect ratio a/b equal to 20, thus the longitudinal direction is much

longer than the transverse one. Consequently, the boundary effects associated to the loaded edges are negligible. The thickness-to-width ratio is 100, and transverse shear effects can be neglected.

Four distinct lay-ups are considered, in order to assess the effect of different elastic couplings on the quality of the semi-analytical predictions. All lay-ups are obtained by stacking four plies because those with more plies tend to exhibit less anisotropy [8]. More specifically, the stacking sequences of the plates are:

- Lay-up 1: $[90°/0°/90°/0°]$

- Lay-up 2: $[0°/0°/0°/90°]$

- Lay-up 3: $[45°/45°/-45°/-45°]$

- Lay-up 4: $[90°/90°/45°/-45°]$

To quantify the elastic coupling due to the plate non-symmetry, a possible measurement is given by the nondimensional parameter η_{B}, defined as:

$$\eta_{\mathrm{B}} = \frac{\lambda^2}{b^2} \frac{e_{12}}{\sqrt[4]{a_{11}a_{22}d_{11}d_{22}}} \tag{66}$$

where λ denotes the number of half-waves of the buckling pattern. The parameter provides a measure of the coupling induced by the term e_{12}, which has a relevant impact on the postbuckling response of axially compressed plates [8].

According to the parameter of Eq. (66), the highest degree of coupling is exhibited by Lay-up 4. Lay-ups 1 and 2 are characterized by a milder coupling, whereas η_{B} is null for Lay-up 3.

All the results are computed by assuming an initial imperfection equal to 1% of the plate thickness and using a number of 15×40 functions, chosen according to a preliminary convergence analysis. The non-dimensional applied load $\frac{N_x}{N_{x,\mathrm{iso}}}$ is reported versus the maximum out of plane deflection in Figure 2. Here, $N_{x,\mathrm{iso}}$ denotes the buckling force per unit length of a plate with a quasi-isotropic laminate.

It is worth highlighting that the closed-form solution of Ref. [8] does not account for the effect of the initial imperfections. This explains the slight difference observed in proximity of the buckling load for the four lay-ups.

Close agreement can be observed in Figures 2(a) and 2(c) between semi-analytical, closed-form

and Abaqus results for the Lay-ups 1 and 3 that are characterized by the smaller amount of anisotropy in terms of the parameter η_B. Contrarily, a slight discrepancy can be observed in Figure 2(b), where the amount of anisotropy is higher in comparison to Lay-ups 1 and 3. In this case, Abaqus and the semi-analytical results are quite close, but describe a stiffer response of the plate in comparison to the prediction of Ref. [8]. This discrepancy is explained recalling that the closed-form solution of Ref. [8] is developed for a single plate, without accounting for the effect of the surrounding structure. For a single plate, the zero moment condition at the four edges promotes the onset of out of plate deflections, whose entity increases with the parameter η_B. On the contrary, for the periodic structure of Figure 1, bending moments along the contour are continuous, but not necessarily zero. Thus, the effect of the zero moment condition is not observed, and the resulting out of plane displacements are smaller. In this sense, the portion of structure surrounding the central plate has a stiffening effect on the plate. This behaviour is more pronounced for Lay-up 4, reported in Figure 2(d), which is the laminate characterized by the highest value of the parameter η_B. In this case, semi-analytical and Abaqus results are in good agreement, while the response predicted in Ref. [8] is drastically different. To further verify the correctness of the results, a finite element simulation is conducted by considering the plate as single entity, thus avoiding the modeling of the surrounding structure. The results are reported in Figure 2(d) and they match well with the predictions of Ref. [8].

The comparisons of Figure 2 allow to conclude that the discrepancies obtained by modeling the structure as a single plate or as part of a periodic structure increase with the degree of anisotropy induced by the laminate non-symmetry. Furthermore, it is important to highlight that the response of a non-symmetric periodic plate tends to be always of bifurcational type. Referring to Figure 2, all the semi-analytical results, which are obtained for a periodic plate, display a bifurcational instability. This consideration holds even in the case of Figure 2(d), where, on the contrary, the single plate displays noticeable pre-buckling deflections and a non-bifurcational instability.

Another response commonly investigated in the postbuckling analysis of structures is the force-shortening curve. For the four lay-ups here investigated, the results are presented in Figure 3. With regard to the quality of the semi-analytical predictions, close matching is observed for all the configurations, except Lay-up 4.

4.2 Comparison with finite element results

To further investigate the potentialities of the semi-analytical approach, the assessment of the results is extended to consider a panel of finite length and exhibiting a complex postbuckling response. In particular, a panel with aspect ratio a/b=1.8 and b/h=100 is considered. The panel is layered with the lay-up $[0°/0°/0°/90°]$ and is loaded with a compressive load. The maximum out of plane displacement is reported in Figure 4 for different load levels, together with the buckled mode predicted using the semi-analytical method and using a Abaqus nonlinear analysis. In the initial loading phase, the panel exhibits a single half-wave along the transverse and longitudinal directions. Then, a sudden change of configuration is experienced by the structure, whose deflected pattern changes from one to three longitudinal half-waves. As observed from Figure 4, semi-analytical and numerical predictions are in close agreement despite the complexity of the postbuckling response of the panel.

The numerical/semi-analytical comparison is presented in terms of force-displacement curve in Figure 5. The initial part of the curve, relative to the pre-buckling field, is almost linear. Then, a progressive, smooth reduction of the stiffness is observed in the postbuckling field, until a sudden snap-back happens at a load level of approximately $N_x/N_{x,\text{iso}}$=2. The snap of the curve is quite sharp and, as seen in Figure 5, is well captured by the semi-analytical method. It is highlighted that the finite element solution, achieved using an arc-length solution procedure, is particularly hard in terms of convergence issues. Several iterations are performed throughout the solution process and a number of preliminary analyses was necessary to avoid premature stopping. On the other hand, the arc-length procedure implemented in the semi-analytical procedure does not reveal any convergence issues, and the analysis is terminated in less than a second of CPU time. Additional comparisons are proposed to further clarify the potentialities of the method. Two panels made of IM7/8552, whose properties are reported in Table 1, are studied with regard to their postbuckling behaviour due to compression and shear loadings. The width-to-thickness ratio is fixed to 100, and the ratio between the longitudinal and the transverse length is equal to 3.

The two panels are layered with lay-ups $[0°/90°/0°/90°]$ and $[0°/90°/45°/-45°]$ and, henceforth, will be denoted as Panel A and Panel B.

The results obtained for the case of pure axial loading are presented in Figures 6-7. In particular,

the out of plane displacements are reported in Figure 6 for different load levels. The good quality of semi-analytical prediction can be appreciated especially for the second configuration, where a relatively complex path is observed due to a postbuckling snapping phenomenon. Good agreement is also visible in Figure 7 in terms of force-displacement curves. Here, the sharp snap-back of the second configuration is clearly seen in the plot of Figure 7(b).

The behaviour of the two panels loaded in shear is illustrated in Figures 8-10.

The maximum out of plane deflection is presented in Figure 8. Abaqus and semi-analytical results are very similar for the cross-ply configuration, while a more pronounced difference is achieved for the second configuration. This discrepancy can be attributed to the highest degree of anisotropy of Panel B in terms of the nondimensional parameter η_{B}. Furthermore, the constitutive law of Panel A is relatively simple due to the cross-ply stacking sequence, while additional terms of elastic couplings characterize the constitutive law of Panel B. It follows that the deflected surface of Panel B has a more complex shape, and its description can be captured with a lower degree of accuracy. It can be noted that, as expected, the Ritz models are always stiffer in comparison to the finite element model due to the lower number of degrees of freedom involved in the approximation of the unknowns.

In any case, the postbuckled pattern is predicted with a satisfactory degree of accuracy in both cases. Figures 9 and 10 illustrate the deformed configurations obtained with the semi-analytical approach and Abaqus nonlinear analyses for two distinct load levels. In particular, Figure 9 is relative to the cross-ply panel, while Figure 10 displays the behaviour of the panel with lay-up [0°/90°/45°/-45°].

In both cases, the semi-analytical method correctly predicts the number of half-waves, three in the first case and two in the second, as well as their skew during the loading process. It can be observed that the increasing skewness experienced by the panel during the loading process is also accurately captured.

Buckling and vibration

Most of the analytical development of the present formulation deals with the nonlinear postbuckling analysis. However, to provide a comprehensive overview of the capabilities of the method, the comparison is presented also in terms of buckling and vibration analysis. A summary of the

results for the Panels A and B is presented in Table 2, where the nondimensional frequencies and buckling loads are presented. The buckling results deal with pure compression and shear loads. Overall, the agreement between numerical and semi-analytical results is very good. The free vibrations are accurately predicted, with percent differences close to zero for both panels. Similarly, the buckling predictions are below 1% for Panel A, i.e. the cross-ply configuration, where the assumption of uniform pre-buckling stress distribution is effectively satisfied. Contrarily, the pre-buckling stress field is not exactly uniform for Panel B, for which higher percent differences are consequently achieved, both in case of compression and shear. In any case, the errors against finite elements are below 5%, and can be still considered an acceptable approximation.

5 Application to design optimization

To illustrate an application of the fast design procedure, the optimal design of two panels is discussed, introducing requirements on the linear and nonlinear response.

A panel with length of 450 mm and width of 150 mm is considered. The laminate is layered with a number of 16 plies, whose elastic properties are those of Table 1, and the overall thickness of the laminate is 2 mm. The optimization problem is presented in the form of a stacking optimization problem, where the design variables are the angles of orientation of the plies. The constraint of balanced laminate is enforced a priori by assuming a stacking sequence with plies at $\pm\theta$, thus reducing the total number of design variables to 8. Each ply is allowed to assume an orientation between $0°$ and $90°$. Two possible angle steps are assumed. In a first optimization the plies are allowed to vary with an angle of $15°$. The total number of possible designs is equal to 7^8, and the optimal configuration is denoted as Opt15. In a second run, the plies can vary with a step of $7.5°$, thus allowing a huge enlargement of the design space to 13^8 combinations (more than 800 million possible designs). In this case, the optimum is denoted as Opt75.

The optimization aims to improve the panel response with respect to a quasi-isotropic baseline with lay-up $[\pm45°/0_2^\circ/90_2^\circ/0_2^\circ]_s$, quantifying the possible benefits due to the adoption of different ply steps. The optimization problem is formulated as the maximization of the linear buckling load subjected to a constraint regarding the first natural frequency and the maximum out of

24

plane displacement in the postbuckling field. In particular, the problem is formulated as:

$$\max P_{\text{buck}}$$

$$\text{subject to:} \quad \begin{cases} \omega > \overline{\omega} \\ w_{\max} > \overline{w}_{\max} \quad \text{at } P = 2.5\overline{P}_{\text{buck}} \end{cases} \tag{67}$$

The overline denotes the reference quantities, which are established by analyzing the baseline configuration. In particular, the first natural frequency of vibration is $\overline{\omega}$=1600 rad/s, while the buckling load is $\overline{P}_{\text{buck}}$=23.1 kN.

The constraint on the maximum out of plane displacement is $\overline{w}_{\max}$ =3.90 mm, and is measured at a load level equal 2.5 times the buckling load. This latest condition ensures that, within the design space under investigation, all the panels are required to work in the postbuckling field. Indeed, the solution of the unconstrained buckling maximization problem identifies the configuration with all the plies at ±45° as the optimal solution and the corresponding buckling load is P_{buck}=27.8 kN. It is important to highlight that the configuration that maximizes the buckling load exhibits a maximum out of plane displacement of 6.98 mm when P=2.5 $\overline{P}_{\text{buck}}$, therefore violating the nonlinear constraint here imposed.

5.1 Optimization results

The results obtained for the two optimizations are here discussed. The parameters to set up the analysis are the same in both cases, apart from the size of the population, which is equal to 30 individuals when the ply step is 15°, and equal to 50 when the step is 7.5°. The number of elite individuals is fixed to 1, so guaranteeing that the best member of each generation is passed intact to the following generation. Fitness scaling is performed using a rank-based strategy, where the fitness is scaled depending on the rank of each individual instead of its score. The stopping criterion is based on the maximum number of generations without improvements. The procedure terminates if the average change in the best fitness function value over 50 generations is less than or equal to a tolerance set of 1e-8. The first optimization terminates after 81 generations, while the second one requires a total of 92 generations to meet the stopping criterion. Considering the numbers of individuals used in the two cases, the overall number of function evaluations is equal to 2430 for the first run and 4600 for the second one. In any case, a reduced computational effort is guaranteed in both cases, thanks to the efficient implementation of the analysis tool. All the

analysis are performed on Core i7 2.30 GHz laptop, with 16 GB of RAM. The computational time to perform the two optimizations is approximately 39 and 77 minutes, respectively. To highlight the benefits associated to the use of the formulation, it is interesting to provide a comparison against the time needed by an equivalent finite element procedure. The estimate is here obtained by considering the analysis time of the reference configuration, and assuming that the same time is needed for each of the configurations analyzed during the optimization process. Conservatively, the time for the mesh generation and the parsing of results are assumed to be null. Under these assumptions, the overall time would be of 38 and 72 hours, and the speedup due to the use of the formulation is then, approximately, 55. The two optimal configurations and the corresponding values of buckling load, first natural frequency and maximum out of plane displacement are summarized in Table 3.

As observed from Table 3, the two optimal solutions satisfy the design constraints and allow an increase of the panel buckling load. The Opt15 is characterized by a buckling load 10.8% higher compared to the baseline. On the other hand, no significant improvement is achieved by enlarging the design space as for the Opt75 design. In this case, the buckling load is 11.7% higher than the baseline, but still very close to the Opt15 configuration.

6   Conclusions

The development of a semi-analytical procedure with postbuckling capabilities has been discussed together with its implementation in the context of an optimization toolbox based on genetic algorithms. The main advantage of the approach is the possibility of considering a wide class of laminates, including those characterized by midplane un-symmetry, in a very efficient manner. The comparison with Abaqus simulations allowed to conclude that the method combines the rapidity typical of closed-form solutions with the accuracy of finite element analyses.

The results have highlighted the effects induced by the non-symmetry of the lamination scheme, illustrating a substantial difference in the response exhibited by single plates and plates operating in the context of periodic structures, as in the case of stiffened panels.

The efficient implementation of the method, which allows to perform a nonlinear analysis in less than a second of computational time, makes it suitable to perform structural optimizations, even when large design spaces are of concern. The speedup against standard finite element-

based procedures is between one and two orders of magnitude and, for this reason, the proposed optimization toolbox can successfully be employed to fully exploit the tailoring opportunities offered by unconventional layups. Two applicative examples have been discussed regarding the buckling maximization of panels layered with 16 plies and ply angles oriented with steps of $7.5°$ and $15°$. The results have illustrated the possibility of improving the buckling load of the structure, while restricting its postbuckling deflections at a given load level. No significant improvement was observed by enlarging the design space from ply steps of $15°$ to $7.5°$, but general conclusions cannot be drawn as loading conditions were restricted to the case of pure compression. The benefits of considering ply steps of $7.5°$ could be more relevant if more complex loading conditions are investigated. In this sense, further investigation is still needed.

References

[1] P. Pevzner, H. Abramovich, and T. Weller. Calculation of the collapse load of an axially compressed laminated composite stringer-stiffened curved panel - an engineering approach. *Composite Structures*, 83(4):341–353, 2008.

[2] C. Bisagni and R. Vescovini. Analytical formulation for local buckling and post-buckling analysis of stiffened laminated panels. *Thin-Walled Structures*, 47(3):318–334, 2009.

[3] Milazzo A and V. Oliveri. Post-buckling analysis of cracked multilayered composite plates by pb-2 Rayleigh–Ritz method. *Composite Structures*, 132:75–86, 2015.

[4] C. Bisagni and R. Vescovini. Fast tool for buckling analysis and optimization of stiffened panels. *Journal of Aircraft*, 46(6):2041–2053, 2009.

[5] R. Vescovini and C. Bisagni. Buckling analysis and optimization of stiffened composite flat and curved panels. *AIAA Journal*, 50(4):904–915, 2012.

[6] R. Chandra. Postbuckling analysis of crossply laminated plates. *AIAA Journal*, 13(10):1388–1389, 1975.

[7] M.-L. Dano and M.W. Hyer. Thermally-induced deformation behavior of unsymmetric laminates. *International Journal of Solids and Structures*, 35(17):2101–2120, 1998.

[8] C.G. Diaconu and P.M. Weaver. Postbuckling of long unsymmetrically laminated composite plates under axial compression. *International Journal of Solids and Structures*, 43(22-23):6978–6997, 2006.

[9] K. Nie, Y. Liu, and Y. Dai. Closed-form solution for the postbuckling behavior of long unsymmetrical rotationally-restrained laminated composite plates under inplane shear. *Composite Structures*, 122:31–40, 2015.

[10] Y. Zhang and F.L. Matthews. Postbuckling behaviour of curved panels of generally layered composite materials. *Composite Structures*, 1(2):115–135, 1983.

[11] J. Zhang, Q. Li, and Y. Shu. Nonlinear stability of unsymmetrically laminated angle-ply shear-deformable plates in biaxial compression. *Thin-Walled Structures*, 38(1):1–16, 2000.

[12] M.S. Qatu and A.W. Leissa. Buckling or transverse deflections of unsymmetrically laminated plates subjected to in-plane loads. *AIAA Journal*, 31(1):189–194, 1993.

[13] V. Giavotto. Sulla meccanica di pannelli di strutture aerospaziali. *Memorie dell' Istituto Lombardo - Accademia di Scienze e Lettere*, XXV(4), 1966. [Italian].

[14] I. Sheinman and Y. Reichman. A study of buckling and vibration of laminated shallow curved panels. *International Journal of Solids and Structures*, 29(11):1329–1338, 1992.

[15] R. Vescovini and C. Bisagni. Semi-analytical buckling analysis of omega stiffened panels under multi-axial loads. *Composite Structures*, 120:285–299, 2015.

[16] E. Byklum and J. Amdahl. A simplified method for elastic large deflection analysis of plates and stiffened panels due to local buckling. *Thin-Walled Structures*, 40(11):925–953, 2002.

[17] P. Buermann, R. Rolfes, J. Tessmer, and M. Schagerl. A semi-analytical model for local post-buckling analysis of stringer- and frame-stiffened cylindrical panels. *Thin-Walled Structures*, 44(1):102–114, 2006.

[18] R. Vescovini and C. Bisagni. Two-step procedure for fast post-buckling analysis of composite stiffened panels. *Computers & Structures*, 128:38–47, 2013.

[19] E. Steen. Application of the perturbation method to plate buckling problems. Technical Report 98-1, University of Oslo, Department of Mathematics, Mechanics Division, 1998.

[20] S. Nagendra, D. Jestin, Z. Gürdal, R.T. Haftka, and L.T. Watson. Improved genetic algorithm for the design of stiffened composite panels. *Computers & Structures*, 58(3):543–555, 1996.

[21] L. Grosset, S. Venkataraman, and R.T. Haftka. Genetic optimization of two-material composite laminates. In *ASC 16th Annual Technical Conference*, Blacksburg, VA, 10–12 September 2011.

Table 1: Material properties of IM7/8552.

	E_{11} (MPa)	E_{22} (MPa)	G_{12} (MPa)	ν_{12}	ρ (kg/m^3)
IM7/8552	150000	9080	5290	0.32	1570

Table 2: Comparison of buckling and eigenfrequency analysis for Panel A and B.

	$\omega \left(\dfrac{b^2}{h}\right) \sqrt{\dfrac{\rho}{E_2}}$			$N_{x,\text{buck}} \dfrac{b^2}{E_2 h^3}$			$N_{xy,\text{buck}} \dfrac{b^2}{E_2 h^3}$		
	Abaqus	Semi-an.	% diff	Abaqus	Semi-an.	% diff	Abaqus	Semi-an.	% diff
Panel A	8.02	8.02	0.00	14.73	14.73	0.00	30.96	31.17	0.68
Panel B	6.13	6.14	0.16	19.13	18.47	3.45	19.56	18.60	4.90

Table 3: Optimization results.

	Layup	P_{buck} [kN]	ω [rad/s]	w_{max} [mm]
Ref. values	$[\pm 45/0_2/90_2/0_2]_s$	23.1	1600	3.87
Opt15	$[\pm 60/\pm 45/\pm 30/\pm 0_2/\pm 30/\pm 45/\pm 60]$	25.6	1913	3.90
Opt75	$[\pm 52.5/\pm 60/\pm 22.5/\pm 7.5_2/\pm 30/\pm 60/\pm 52.5]$	25.8	1909	3.78
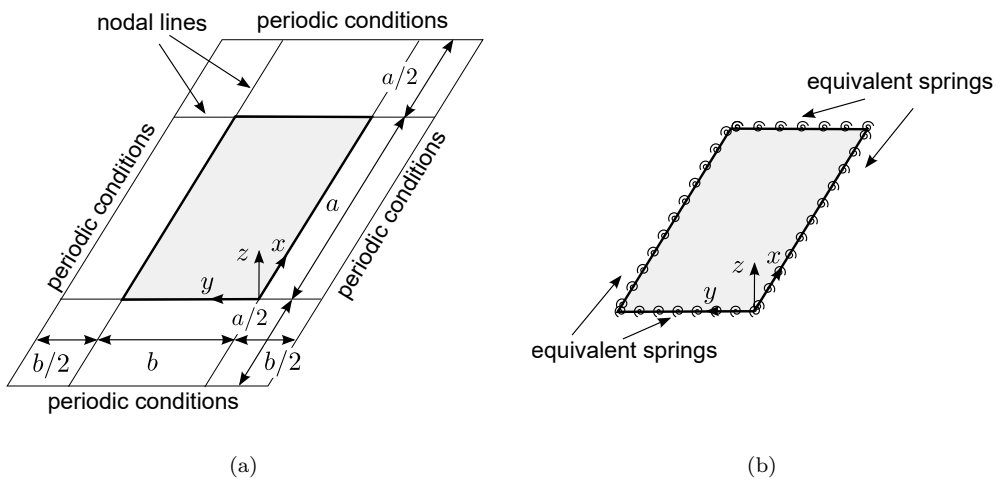
Figure 1: Panel geometry and reference system: (a) representative unit used for linear buckling analysis, (b) reduced model used for postbuckling analysis.
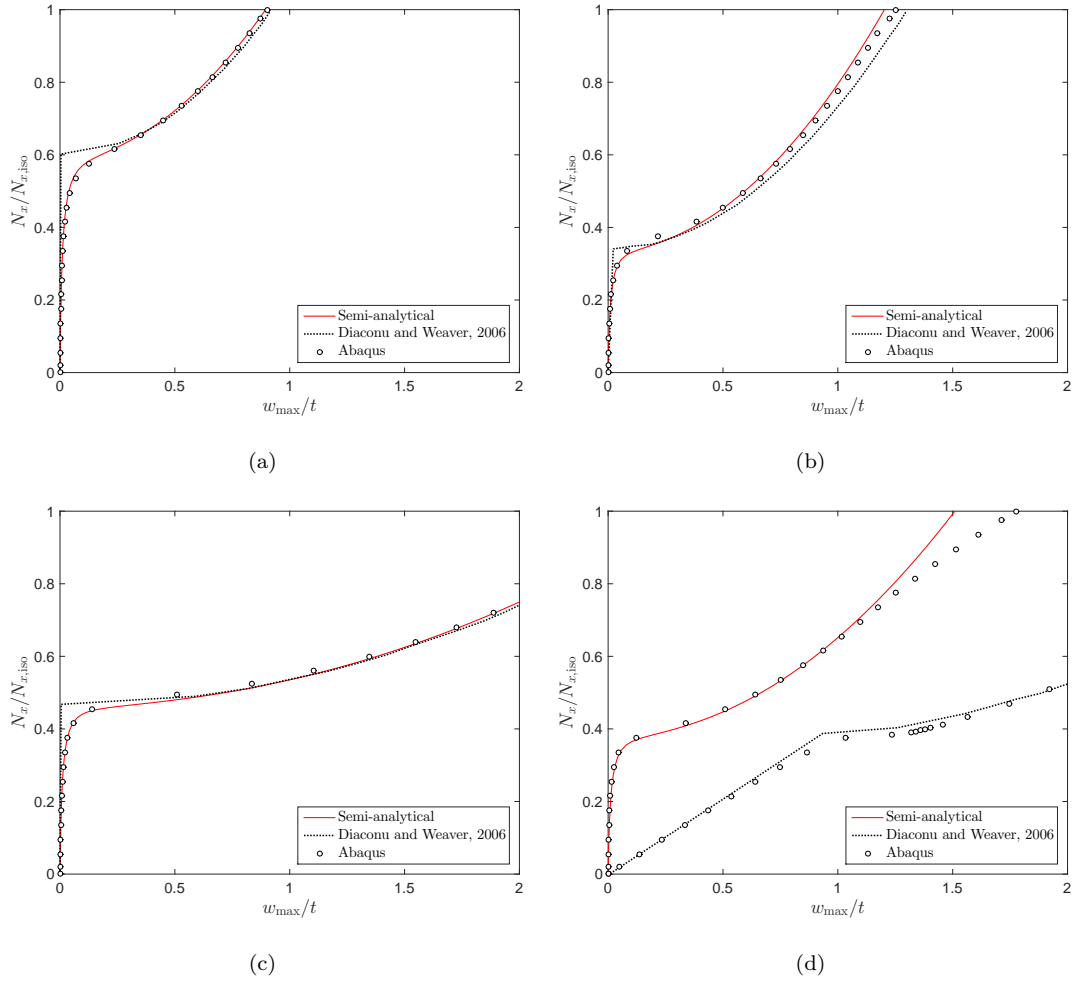
Figure 2: Curves of nondimensional load per unit length versus maximum out of plane displacement for panels with a/b=20 and different lay-ups: (a) $[90°/0°/90°/0°]$, (b) $[0°/0°/0°/90°]$, (c) $[45°/45°/-45°/-45°]$, (d) $[90°/90°/45°/-45°]$.
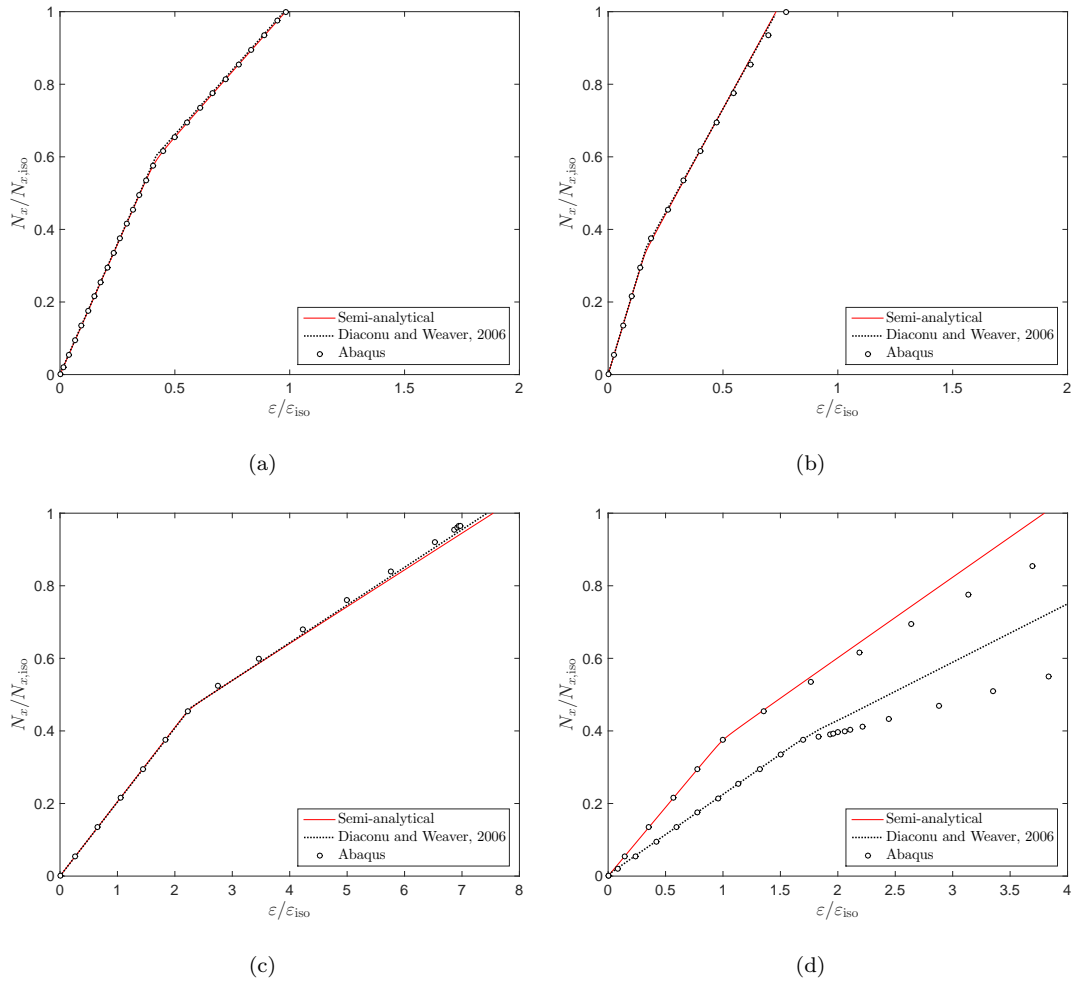
Figure 3: Curves of nondimensional load per unit length versus axial strain for panels with a/b=20 and different lay-ups: (a) $[90°/0°/90°/0°]$, (b) $[0°/90°/90°/90°]$, (c) $[45°/45°/-45°/-45°]$, (d) $[90°/90°/45°/-45°]$.
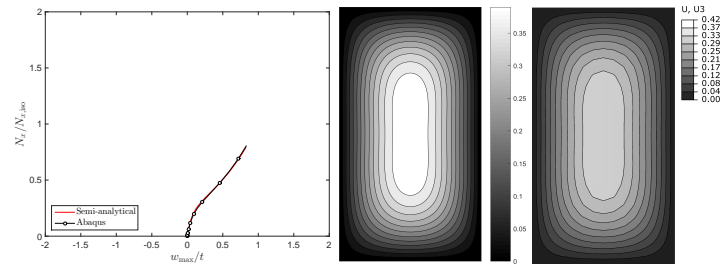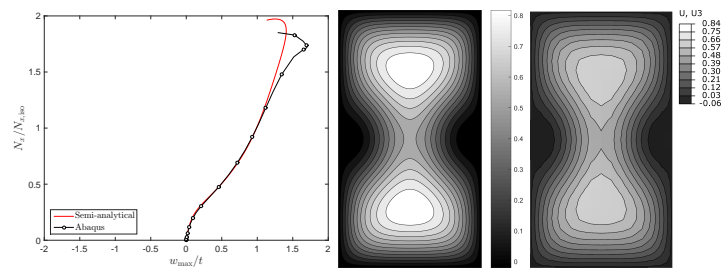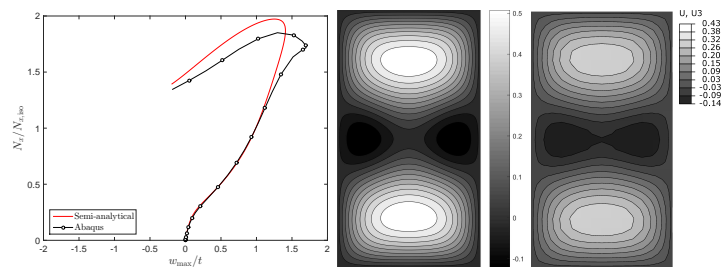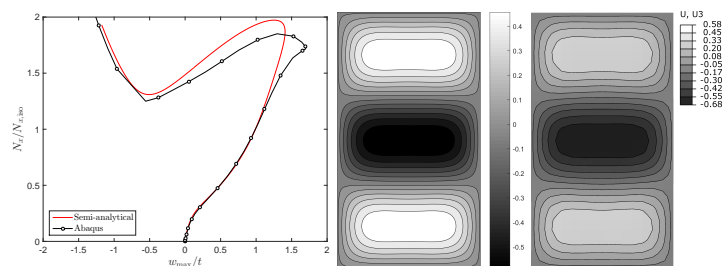
Figure 4: Panel with a/b=1.8 and lay-up [90°/0°/90°/0°]. Behaviour at: (a) initial postbuckling range, (b) beginning of the unloading phase, (c) unloading phase, (d) deep-post buckling field, after mode transition.
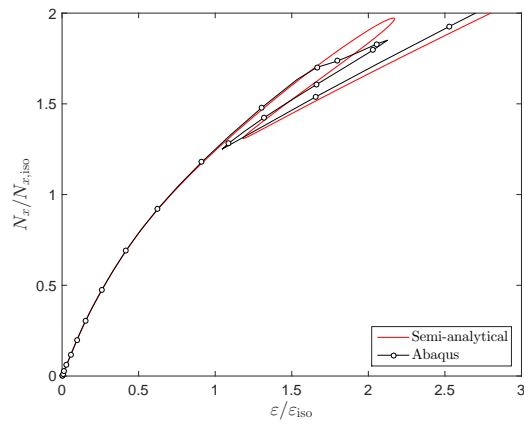
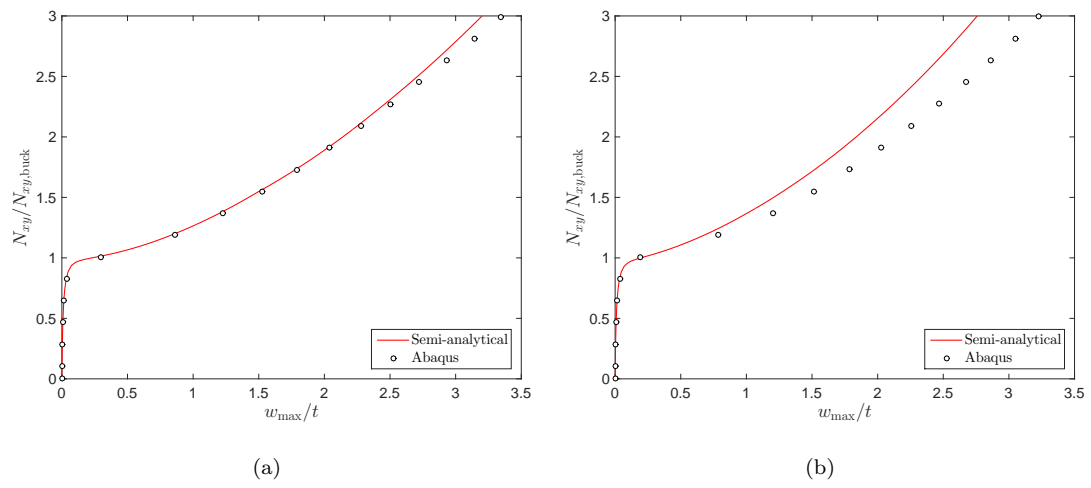Figure 5: Nondimensional load per unit length versus axial strain for panel with a/b=1.8 and lay-up $[90°/0°/90°/0°]$.
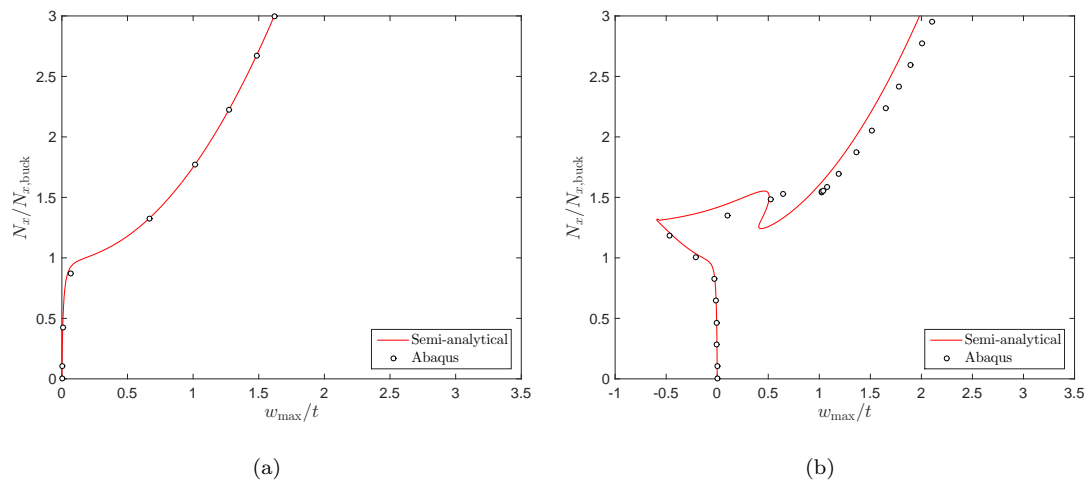
Figure 6: Nondimensional load per unit length versus out of plane displacement for panels loaded in compression with lay-up: (a) $[0°/90°/0°/90°]$, (b) $[0°/90°/45°/\text{-}45°]$.
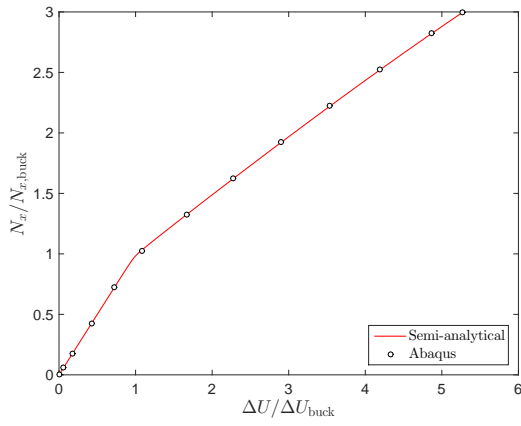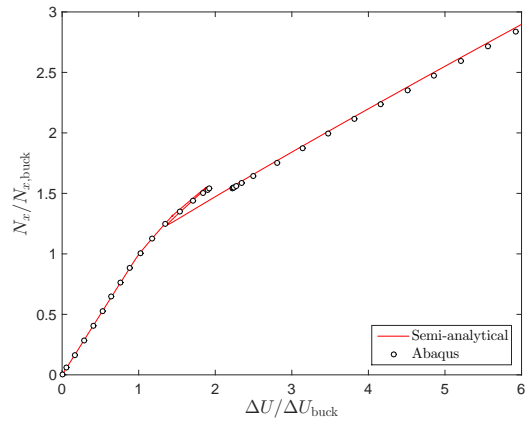
Figure 7: Nondimensional load per unit length versus versus axial shortening for panels loaded in compression with lay-up: (a) $[0°/90°/0°/90°]$, (b) $[0°/90°/45°/-45°]$.

Figure 8: Nondimensional load per unit length versus out of plane displacement for panels loaded in shear with lay-up: (a) $[0°/90°/0°/90°]$, (b) $[0°/90°/45°/-45°]$.
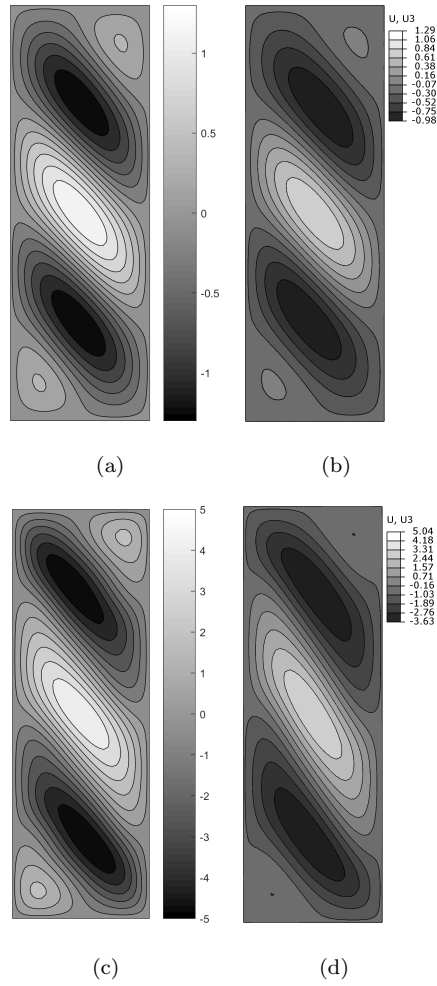
Figure 9: Contour of out of displacements for Panel A: (a) initial postbuckling, semi-analytical, (b) initial postbuckling, Abaqus, (c) deep postbuckling, semi-analytical, (d) deep postbuckling, Abaqus.
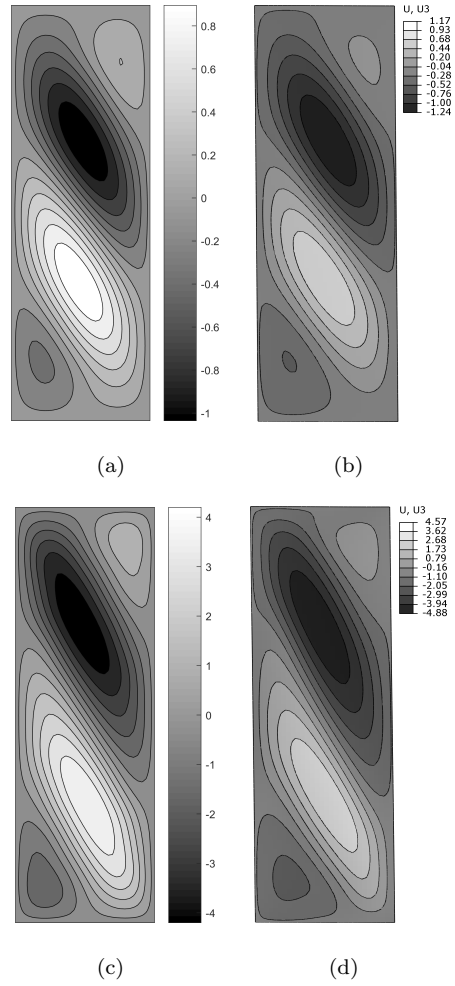
Figure 10: Contour of out of displacements for Panel B: (a) initial postbuckling, semi-analytical, (b) initial postbuckling, Abaqus, (c) deep postbuckling, semi-analytical, (d) deep postbuckling, Abaqus.